J. Fluid Mech. (2008), *vol.* 613, *pp.* 125–134. © 2008 Cambridge University Press
doi:10.1017/S002211200800356X Printed in the United Kingdom

Tensorial hydrodynamic slip

MARTIN Z. BAZANT[1,3] AND OLGA I. VINOGRADOVA[2,3]

[1]Department of Mathematics, Massachusetts Institute of Technology, Cambridge, MA 02139, USA
[2]A. N. Frumkin Institute of Physical Chemistry and Electrochemistry, Russian Academy of Sciences, 31 Leninsky Prospect, 119991 Moscow, Russia
[3]CNRS UMR Gulliver 7083 and PMMH 7636, École Supérieure de Physique et de Chimie Industrielles, 10 rue Vauquelin, F-75005 Paris, France

(Received 13 June 2007 and in revised form 27 July 2008)

We describe a tensorial generalization of the Navier slip boundary condition and illustrate its use in solving for flows around anisotropic textured surfaces. Tensorial slip can be derived from molecular or microstructural theories or simply postulated as a constitutive relation, subject to certain general constraints on the interfacial mobility. The power of the tensor formalism is to capture complicated effects of surface anisotropy, while preserving a simple fluid domain. This is demonstrated by exact solutions for laminar shear flow and pressure-driven flow between parallel plates of arbitrary and different textures. From such solutions, the effects of rotating a texture follow from simple matrix algebra. Our results may be useful for extracting local slip tensors from global measurements, such as the permeability of a textured channel or the force required to move a patterned surface, in experiments or simulations.

1. Introduction

The emergence of microfluidics has focused renewed attention on hydrodynamic boundary conditions (Stone, Stroock & Ajdari 2004). Reducing fluid volumes enhances the impact of surface phenomena (Squires & Quake 2005), so the use of appropriate boundary conditions is crucial to the design and optimization of lab-on-a-chip devices. It is now widely recognized that the classical no-slip hypothesis supported by macroscopic experiments does not always apply at the micro- and, especially, the nano-scale.

In this context, the phenomenon of liquid slip at solid surfaces has been studied extensively in experiments, theoretical calculations, and simulations (Vinogradova 1999; Lauga, Brenner & Stone 2007; Bocquet & Barrat 2007). The results are usually interpreted in terms of the Navier boundary condition,

$$\Delta u = u - U = b\,\frac{\partial u}{\partial n} \tag{1.1}$$

where the fluid velocity u minus the surface velocity U is proportional to the shear strain rate $\partial u/\partial n$ via the slip length b. Flow past smooth hydrophilic surfaces has been shown to be consistent with the no-slip hypothesis, but b can reach tens of nanometres for hydrophobic surfaces (Vinogradova & Yakubov 2003; Cottin-Bizonne *et al.* 2005; Joly, Ybert & Bocquet 2006). Hydrophobicity can be significantly amplified by roughness and can reduce friction due to trapped nanobubbles (Vinogradova *et al.* 1995; Cottin-Bizonne *et al.* 2003). Extreme hydrophobicity can be generated with well-controlled textures (Quéré 2005), leading to a many-micron slip lengths (Ou & Rothstein 2005; Joseph *et al.* 2006; Choi *et al.* 2006) and very fast transport of water

https://doi.org/10.1017/S002211200800356X Published online by Cambridge University Press

through microchannels. The strong anisotropy of such surfaces, however, can limit the validity of (1.1).

The possibility of transverse flow over a grooved no-slip surface, perpendicular to an applied shear stress, has been analysed by Stroock *et al.* (2002*b*), Ajdari (2002), and Wang (2003) and exploited for chaotic mixing in microfluidic devices by Stroock *et al.* (2002*a*). In this context, Stroock *et al.* (2002*b*) expressed the permeability $\boldsymbol{\kappa}$ of a thin parallel-plate microchannel with one grooved and one flat surface in terms of an effective *slip-length tensor*, $\boldsymbol{b} = \{b_{ij}\}$, defined by a generalized Navier boundary condition

$$\Delta \boldsymbol{u} = \boldsymbol{u} - \boldsymbol{U} = \boldsymbol{b}(\hat{\boldsymbol{n}} \cdot \nabla \boldsymbol{u}) \tag{1.2}$$

and Stone *et al.* (2004) expressed the velocity profile in terms of $\boldsymbol{b}$. This elegant construction relating permeability to slip, however, assumes that the *global* flow has the same anisotropy as the grooved surface (i.e. $\boldsymbol{\kappa}$ and $\boldsymbol{b}$ are coaxial). This is generally not the case with multiple textured surfaces (Wang 2003), curved walls (Einzel, Panzer & Liu 1990), obstacles in the flow, etc., and we are not aware of any other use of the tensorial relation (1.2). Wang (2003) considered flow between misaligned, grooved plates using (1.2) in component form but deemed the solution 'too tedious to reproduce'. We shall see that this problem and others have very simple solutions in tensorial form.

In this paper, we propose the use of (1.2) as a *local* boundary condition for any surface whose texture perturbs fluid flow on length scales much smaller than the geometry. In § 2 we discuss a general boundary condition relating slip velocity to normal traction via an interfacial mobility tensor. To illustrate its use, we derive exact solutions for two types of laminar flow between textured parallel plates (which can also be superimposed): (i) shear flow due to moving plates in § 3, and (ii) pressure-driven flow in § 4. We close in § 5 by suggesting further applications.

2. Theory

2.1. *The interfacial mobility tensor*

Although (1.1) is the most commonly used boundary condition for hydrodynamic slip, it is not widely known that Navier (1823) also postulated the more general relation

$$\Delta u = M\tau \tag{2.1}$$

where τ is the local shear stress (normal traction) and M is a constant interfacial mobility (velocity per surface stress). For a Newtonian fluid, $\tau = \eta \partial u/\partial n$, this reduces to (1.1) with $b = M\eta$, where η is the viscosity. Molecular dynamics simulations have shown that (2.1) with constant M is more robust than (1.1) with constant b, since the fluctuating slip velocity correlates better with the shear stress (normal forces) than with velocity gradients very close to the surface (Hess & Loose 1989; Bocquet & Barrat 2007).

A natural generalization of the slip condition (2.1) is

$$\Delta \boldsymbol{u} = \boldsymbol{M}(\hat{\boldsymbol{n}} \cdot \boldsymbol{\sigma}) \tag{2.2}$$

where $\hat{\boldsymbol{n}} \cdot \boldsymbol{\sigma} = \boldsymbol{f}_n$ is the fluid force (normal traction) on the interface, $\boldsymbol{\sigma}$ is the local stress tensor, and $\boldsymbol{M}$ is an interfacial mobility tensor. As shown in figure 1, the effective slip vector is generally misaligned with the force vector for an anisotropic surface. Equation (1.2) is recovered with $\boldsymbol{b} = \boldsymbol{M}\eta$ in the case of a Newtonian fluid of viscosity η. For anisotropic surfaces, the mobility is a second-rank tensor $\boldsymbol{M} = \{M_{ij}\}$, whether the averaging of surface forces occurs over microstructural or molecular heterogeneity.

https://doi.org/10.1017/S002211200800356X Published online by Cambridge University Press

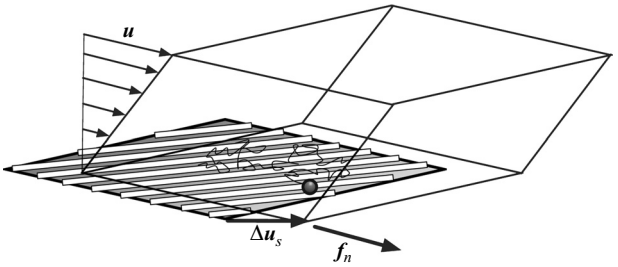


FIGURE 1. Physical picture of tensorial slip. The normal traction $\boldsymbol{f}_n$ exerted by the fluid on an anisotropic surface produces an effective slip velocity $\Delta\boldsymbol{u} = \boldsymbol{M}\,\boldsymbol{f}_n$ in a different direction. At the molecular level, the interfacial mobility tensor $\boldsymbol{M}$ can be related to trajectories of diffusing interfacial particles, such as the one shown.

As with scalar slip (Bocquet & Barrat 2007), the tensorial slip boundary condition (2.1) can be justified in various ways. At the microstructural level, grooved surfaces (with or without scalar slip) have effective tensorial slip coefficients, which can be explicitly calculated for simple geometries, if the grooves vary on much smaller scales than the fluid domain (Stroock *et al.* 2002*b*; Wang 2003). At the molecular level, nanoscale surface anisotropy has a similar effect, but due to statistical interactions.

A possible starting point for molecular modelling is a tensorial Einstein relation, $\boldsymbol{D} = \boldsymbol{M}kT/S$, relating $\boldsymbol{M}$ to the 'interfacial diffusivity' per unit area S, by analogy with the theory of Brownian motion. This yields the statistical formula

$$M_{ij} = \frac{S}{2kT} \lim_{t\to\infty} \frac{\mathrm{d}}{\mathrm{d}t} \operatorname{Cov}(\Delta x_i(t),\, \Delta x_j(t)) \tag{2.3}$$

where $\Delta\boldsymbol{x}(t) = \boldsymbol{x}(t) - \boldsymbol{U}t$ is the fluctuating position of an interfacial fluid molecule, in a frame moving with the mean surface velocity (figure 1), where the 'interface' may include molecules distinct from the bulk fluid, e.g. in a vapour phase. Observing thermal diffusion near a surface to infer its slip length was also exploited in experiments by Joly *et al.* (2006). The mobility formula (2.3) can be recast in a tensorial Green–Kubo form,

$$M_{ij} = \frac{S}{kT} \int_0^\infty \mathrm{d}t\, \operatorname{Cov}(v_i(0),\, v_j(t)) \tag{2.4}$$

where $\boldsymbol{v}(t) = \mathrm{d}\Delta\boldsymbol{x}/\mathrm{d}t$. These formal expressions assume convergence in the thermodynamic limit (taken before $t \to \infty$) for molecular trajectories exploring the interfacial region on scales much larger than the surface heterogeneity. In that case, via the covariance matrix, $\boldsymbol{M}$ is symmetric, positive definite and thus invertible. As noted by Bocquet & Barrat (2007), the inverse mobility, or friction tensor $\boldsymbol{F} = \boldsymbol{M}^{-1}$, also has a tensorial Green–Kubo representation, as the integral of the auto-correlation function for forces exerted by the fluid on the surface (Bocquet & Barrat 1994).

2.2. *General properties of* $\boldsymbol{M}$

Regardless of its microscopic justification, we suggest adopting (2.2) as a general, interfacial constitutive relation for continuum mechanics. Like its bulk counterpart relating the stress and deformation rate, its form can be either derived from microscopic models or simply postulated and fit to experimental data, subject to certain constraints discussed below. For a general 'nonlinear interface', the mobility tensor $\boldsymbol{M}$ could depend on the surface forces, as well as internal degrees of freedom, such as the local orientation of surface molecules or deformable microstructures; for

https://doi.org/10.1017/S002211200800356X Published online by Cambridge University Press

example, hinge-like structures could lead to different slip in opposite directions. For permeable surfaces with $\hat{\boldsymbol{n}} \cdot \Delta \boldsymbol{u} \neq 0$, the mobility tensor may be represented by a 3×3 matrix with tangential–normal couplings, a possibility which has not been considered before to our knowledge.

Here, we will focus on the simplest case of impermeable, macroscopically homogeneous, linear interfaces, where $\boldsymbol{M}$ is a constant 2×2 matrix in a local suitable coordinate system of the tangent plane. Below we will refer to the mobility tensor as defining the 'texture' of a surface up to a rotation, which sets the 'orientation'. The tensor formalism allows us to easily change the orientation of a texture, once a problem has been solved in terms of mobility tensors for a given geometry. The mobility simply transforms as

$$\boldsymbol{M} \mapsto \boldsymbol{S}_\theta \, \boldsymbol{M} \, \boldsymbol{S}_{-\theta} \quad \text{where} \quad S_\theta = \begin{pmatrix} \cos\theta & \sin\theta \\ -\sin\theta & \cos\theta \end{pmatrix} \tag{2.5}$$

is a matrix rotating the tangent plane by an angle θ.

We also consider 'passive' surfaces, which do not transfer energy to the fluid. In that case, enforcing a positive rate of work w_I on the slipping interface ($\boldsymbol{M} \neq \boldsymbol{0}$),

$$w_I = \boldsymbol{f}_n \cdot \Delta \boldsymbol{u} = \boldsymbol{f}_n \cdot \boldsymbol{M} \, \boldsymbol{f}_n > 0, \tag{2.6}$$

for any loading $\boldsymbol{f}_n = \hat{\boldsymbol{n}} \cdot \boldsymbol{\sigma}$ implies that $\boldsymbol{M}$ must be positive definite. This argument is similar to the constraint of positive entropy production at a slipping boundary in irreversible thermodynamics (Heidenreich, Ilg & Hess 2007). The statistical arguments above lead to the same conclusion, e.g. since the diffusivity $\boldsymbol{D}$ is positive definite for a passive surface. The eigenvectors of $\boldsymbol{M}$ correspond to special directions along which fluid forces do not produce transverse slip, and the (positive) eigenvalues are the corresponding directional mobilities. Since positive-definite matrices are invertible, the boundary condition can also be expressed as $\boldsymbol{f}_n = \boldsymbol{F} \, \Delta \boldsymbol{u}$ in terms of the (coaxial) friction tensor, $\boldsymbol{F} = \boldsymbol{M}^{-1}$.

Diagonalization allows us to relate $\boldsymbol{M}$ to the position of the slip plane in (2.2), which is independent of the force $\boldsymbol{f}_n$. In each eigendirection $\hat{\boldsymbol{e}}_i$, the tensorial boundary condition (2.2) reduces to the scalar case (2.1), and the eigenvalue M_i depends on the (arbitrary) choice of slip plane in the usual way (Bocquet & Barrat 2007); for a Newtonian fluid (1.1), the slip length $b_i = M_i \eta$ is the position of the slip plane, relative to the (unique) depth of no slip extrapolated from a homogeneous bulk shear flow. By appropriately shifting the eigenvalues $\{M_i\}$, the same slip plane can be chosen for all directions. The mobility tensor is then constructed from the spectral decomposition, $\boldsymbol{M} = \boldsymbol{S}\hat{\boldsymbol{M}}\boldsymbol{S}^{-1}$, where $\hat{\boldsymbol{M}}$ is the diagonal matrix of eigenvalues and $\boldsymbol{S}$ the matrix of column eigenvectors.

2.3. *Symmetric mobility tensors*

Although we will make no further assumptions in our analysis below, a constant mobility tensor is usually symmetric, $M_{ij} = M_{ji}$, as in the statistical formulae above. This is also the case for the effective slip tensor derived by averaging linear Stokes flows over grooved no-slip surfaces (Stroock *et al.* 2002*a*; Wang 2003). More generally, symmetry of $\boldsymbol{M}$ exemplifies the widely used Onsager–Casimir relations of linear response near thermal equilibrium (Bocquet & Barrat 1994; Ajdari 2002; Heidenreich *et al.* 2007).

A 2×2 interfacial mobility matrix, which is symmetric and positive definite, has some useful mathematical properties. There always exists a rotation of the orthogonal

https://doi.org/10.1017/S002211200800356X Published online by Cambridge University Press

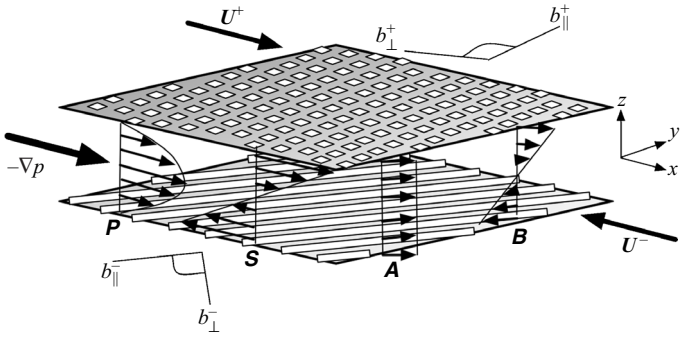


FIGURE 2. Sketch of a fluid region $|z| < h/2$ between upper (+) and lower (−) parallel plates with arbitrary textures (grooves, surface coatings, bubbles, etc.). The texture length scales are much less than the gap h, so each surface has a well defined slip-length tensor, $\boldsymbol{b}^+$ and $\boldsymbol{b}^-$, with eigenvalues $b_\parallel^\pm$ (and $b_\perp^\pm$) in the fastest (and slowest) slipping directions indicated. The plates move at relative velocity $\boldsymbol{U}$ and/or a uniform pressure gradient $-\nabla p$ is applied. In addition to the usual no-slip parabolic Poiseuille flow $\boldsymbol{P}$ and linear shear flow $\boldsymbol{S}$, slip-driven plug-flow $\boldsymbol{A}$ and shear-flow $\boldsymbol{B}$ are superimposed in different directions.

(x, y) coordinate system of the tangent plane $\boldsymbol{S}_\theta$, which diagonalizes the mobility,

$$\boldsymbol{M} = \boldsymbol{S}_\theta \begin{pmatrix} M_\parallel & 0 \\ 0 & M_\perp \end{pmatrix} \boldsymbol{S}_{-\theta} = \begin{pmatrix} M_\parallel \cos^2\theta + M_\perp \sin^2\theta & (M_\parallel - M_\perp)\sin\theta\cos\theta \\ (M_\parallel - M_\perp)\sin\theta\cos\theta & M_\parallel \sin^2\theta + M_\perp \cos^2\theta \end{pmatrix}, \tag{2.7}$$

where $M_\parallel \geqslant M_\perp > 0$ are the eigenvalues. The decomposition $\boldsymbol{M} = M_\parallel \hat{\boldsymbol{e}}_\parallel \hat{\boldsymbol{e}}_\parallel^T + M_\perp \hat{\boldsymbol{e}}_\perp \hat{\boldsymbol{e}}_\perp^T$ shows that $\Delta\boldsymbol{u}$ is a linear superposition of scalar slip in the eigendirections.

Regardless of the complexity of the texture, as long as (2.2) holds at the geometrical scale with a symmetric, positive-definite $\boldsymbol{M}$, there exist orthogonal directions on the surface, $\hat{\boldsymbol{e}}_\parallel = \boldsymbol{S}_\theta \hat{\boldsymbol{x}}$ and $\hat{\boldsymbol{e}}_\perp = \boldsymbol{S}_\theta \hat{\boldsymbol{y}}$, along which there are no transverse hydrodynamic couplings, $\hat{\boldsymbol{e}}_\perp \cdot \boldsymbol{M}\hat{\boldsymbol{e}}_\parallel = 0$. The mobility for 'forward' slip aligned with forcing in a particular direction $\hat{\boldsymbol{e}} = \boldsymbol{S}_\phi \hat{\boldsymbol{x}}$ is given by $\hat{\boldsymbol{e}} \cdot \boldsymbol{M}\hat{\boldsymbol{e}} = M_\parallel \cos^2(\theta - \phi) + M_\perp \sin^2(\theta - \phi)$ and is bounded by the eigenvalues, $M_\perp \leqslant \hat{\boldsymbol{e}} \cdot \boldsymbol{M}\hat{\boldsymbol{e}} \leqslant M_\parallel$. The 'fast' axis of greatest forward slip ($\theta = 0$) is always perpendicular to the 'slow' axis of least forward slip ($\theta = \pi/2$).

2.4. *Simple examples*

In the following sections, we focus on passive linear interfaces and Newtonian fluids, described by the Navier–Stokes equations

$$\rho\left(\frac{\partial \boldsymbol{u}}{\partial t} + \boldsymbol{u}\cdot\nabla\boldsymbol{u}\right) = -\nabla p + \eta\nabla^2\boldsymbol{u} \quad \text{and} \quad \nabla\cdot\boldsymbol{u} = 0. \tag{2.8}$$

In that case, all the properties of $\boldsymbol{M}$ above are inherited by the slip-length tensor, $\boldsymbol{b} = \boldsymbol{M}\eta$, with eigenvalues, $b_\parallel = M_\parallel \eta$ and $b_\perp = M_\perp \eta$. We also assume impermeable, macroscopically homogeneous surfaces, for which $\boldsymbol{b}$ is a constant 2×2 matrix.

To illustrate the use of slip tensors, we consider the geometry in figure 2 where the fluid is confined between flat plates at $z = \pm h/2$ moving at velocities $\boldsymbol{U}^\pm$ (§ 3) or forced by a pressure gradient (§ 4). Each plate has a fine texture (varying on scales $\ll h$) and exhibits uniform tensorial slip,

$$\boldsymbol{u} = \boldsymbol{U}^\pm \mp \boldsymbol{b}^\pm \frac{\partial \boldsymbol{u}}{\partial z} \quad \text{for} \quad z = \pm\frac{h}{2}, \tag{2.9}$$

https://doi.org/10.1017/S002211200800356X Published online by Cambridge University Press

where the slip-length tensors, $\boldsymbol{b}^+$ and $\boldsymbol{b}^-$, are represented by constant, positive-definite (but not necessarily symmetric) 2×2 matrices in the (x, y) coordinate system.

3. Example: shear flow

3.1. *General solution*

The simplest solution of (2.8)–(2.9) corresponds to laminar shear flow between two moving textured plates, shown in figure 2. In terms of the depth-averaged velocity $\overline{\boldsymbol{U}} = (\boldsymbol{U}^+ + \boldsymbol{U}^-)/2$ and relative plate velocity $\boldsymbol{v} = \boldsymbol{U}^+ - \boldsymbol{U}^-$, we can express the solution as

$$\boldsymbol{u} = \overline{\boldsymbol{U}} + \left[\boldsymbol{A}_s + (\boldsymbol{B}_s + \boldsymbol{I})\frac{2z}{h}\right]\frac{\boldsymbol{v}}{2} \tag{3.1}$$

where $\boldsymbol{A}_s$ and $\boldsymbol{B}_s$ are dimensionless 2×2 matrices with the following physical interpretations. The first term in (3.1) describes a slip-driven plug flow in the $\boldsymbol{A}_s\boldsymbol{v}$-direction, and the second describes a slip-driven linear shear flow in the $\boldsymbol{B}_s\boldsymbol{v}$-direction. Substituting (3.1) into (2.9), we find

$$\boldsymbol{A}_s = -\boldsymbol{D}(\boldsymbol{I} + \boldsymbol{C})^{-1} \quad \text{and} \quad \boldsymbol{B}_s = (\boldsymbol{I} + \boldsymbol{C})^{-1} - \boldsymbol{I}, \tag{3.2}$$

where

$$h\boldsymbol{C} = \boldsymbol{b}^+ + \boldsymbol{b}^- \quad \text{and} \quad h\boldsymbol{D} = \boldsymbol{b}^+ - \boldsymbol{b}^-. \tag{3.3}$$

The slip-driven plug flow vanishes ($\boldsymbol{A}_s = \boldsymbol{0}$) only if the textures are the same ($\boldsymbol{D} = \boldsymbol{0}$), and slip-driven shear flow always occurs ($\boldsymbol{B}_s \neq \boldsymbol{0}$, if $\boldsymbol{b}^+ \neq 0$ or $\boldsymbol{b}^- \neq 0$).

The solution (3.1)–(3.2) exists for any $\boldsymbol{b}^\pm$, as long as $\boldsymbol{I} + \boldsymbol{C}$ is invertible; this is ensured for passive surfaces, since $\boldsymbol{b}^\pm$ and $\boldsymbol{C}$ are positive definite, and possible for some active surfaces. In the typical case of symmetric $\boldsymbol{b}^\pm$, the solution can be expressed in terms of the texture orientation angles $\theta^\pm$ and slip-length eigenvalues, $b_\parallel^\pm = M_\parallel^\pm \eta$ and $b_\perp^\pm = M_\perp^\pm \eta$ using (2.7). This can be easily accomplished in the following general situations by diagonalizing $\boldsymbol{A}_s$ and $\boldsymbol{B}_s$.

3.2. *Aligned but different textures*

We first consider 'aligned' surfaces with the same orientation $\theta^\pm = \theta$, but arbitrary slip-length eigenvalues:

$$\boldsymbol{b}^\pm = \boldsymbol{S}_\theta \begin{pmatrix} b_\parallel^\pm & 0 \\ 0 & b_\perp^\pm \end{pmatrix} \boldsymbol{S}_{-\theta}. \tag{3.4}$$

The coefficient tensors (3.2) are then diagonalized by the same rotation matrix

$$\boldsymbol{A}_s = \boldsymbol{S}_\theta \begin{pmatrix} A_s(b_\parallel^+, b_\parallel^-) & 0 \\ 0 & A_s(b_\perp^+, b_\perp^-) \end{pmatrix} \boldsymbol{S}_{-\theta}, \tag{3.5}$$

$$\boldsymbol{B}_s = \boldsymbol{S}_\theta \begin{pmatrix} B_s(b_\parallel^+, b_\parallel^-) & 0 \\ 0 & B_s(b_\perp^+, b_\perp^-) \end{pmatrix} \boldsymbol{S}_{-\theta}, \tag{3.6}$$

and the eigenvalues

$$A_s(b^+, b^-) = -\frac{b^+ + b^-}{h + b^+ + b^-} \quad \text{and} \quad B_s(b^+, b^-) = -\frac{b^+ - b^-}{h + b^+ + b^-} \tag{3.7}$$

result from scalar slip in the eigendirections.

https://doi.org/10.1017/S0022112008003564 Published online by Cambridge University Press

3.3. *Identical but misaligned textures*

Next we consider identical textures with arbitrary orientations, $\theta^{\pm} = \bar{\theta} \pm \Delta\theta$:

$$\boldsymbol{b}^{\pm} = \boldsymbol{S}_{\theta^{\pm}} \begin{pmatrix} b_{\parallel} & 0 \\ 0 & b_{\perp} \end{pmatrix} \boldsymbol{S}_{-\theta^{\pm}}. \tag{3.8}$$

By expressing the sum and difference matrices (3.3) as

$$h\boldsymbol{C} = 2\boldsymbol{S}_{\bar{\theta}} \begin{pmatrix} b_{\parallel}\cos^2\Delta\theta + b_{\perp}\sin^2\Delta\theta & 0 \\ 0 & b_{\parallel}\sin^2\Delta\theta + b_{\perp}\cos^2\Delta\theta \end{pmatrix} \boldsymbol{S}_{-\bar{\theta}}, \tag{3.9}$$

$$h\boldsymbol{D} = \boldsymbol{S}_{\bar{\theta}} \begin{pmatrix} 0 & (b_{\parallel} - b_{\perp})\sin 2\Delta\theta \\ (b_{\parallel} - b_{\perp})\sin 2\Delta\theta & 0 \end{pmatrix} \boldsymbol{S}_{-\bar{\theta}}, \tag{3.10}$$

we find $\boldsymbol{A}_s = \boldsymbol{0}$ and

$$\boldsymbol{B}_s = \boldsymbol{S}_{\bar{\theta}} \begin{pmatrix} -\dfrac{b_{\parallel}\cos^2\Delta\theta + b_{\perp}\sin^2\Delta\theta}{h/2 + b_{\parallel}\cos^2\Delta\theta + b_{\perp}\sin^2\Delta\theta} & 0 \\ 0 & -\dfrac{b_{\parallel}\sin^2\Delta\theta + b_{\perp}\cos^2\Delta\theta}{h/2 + b_{\parallel}\sin^2\Delta\theta + b_{\perp}\cos^2\Delta\theta} \end{pmatrix} \boldsymbol{S}_{-\bar{\theta}}. \tag{3.11}$$

The slip-driven plug flow vanishes by symmetry, and the slip-driven shear flow coefficient $\boldsymbol{B}_s$ is diagonalized by $\boldsymbol{S}_{\bar{\theta}}$, where $\bar{\theta}$ is the angle that bisects the orientation angles. As expected by symmetry, if the two textures are the same (but misaligned), then shearing in this direction cannot produce any transverse flow.

4. Example: pressure-driven flow

4.1. *General solution*

Another simple solution to (2.8)–(2.9) describes steady, laminar flow in response to an applied pressure gradient, $\boldsymbol{g} = -\nabla p = g_x\hat{\boldsymbol{x}} + g_y\hat{\boldsymbol{y}}$, between stationary textured plates in figure 2. We express the solution in the form

$$\boldsymbol{u} = \frac{h^2}{4\eta}\left\{\frac{1}{2}\left[1 - \left(\frac{2z}{h}\right)^2\right]\boldsymbol{I} + \boldsymbol{A}_p + \left(\frac{2z}{h}\right)\boldsymbol{B}_p\right\}\boldsymbol{g} \tag{4.1}$$

where $\boldsymbol{A}_p$ and $\boldsymbol{B}_p$ are dimensionless 2×2 matrices. In spite of surface anisotropy, the velocity is horizontal ($\hat{\boldsymbol{z}} \cdot \boldsymbol{u} = 0$) and varies only in the vertical z-direction, due to translational invariance. The solution (4.1) is a linear superposition of three terms: the familiar parabolic profile of Poiseuille flow in the $\boldsymbol{g}$-direction between parallel no-slip planes; a slip-driven plug flow in the $\boldsymbol{A}_p\boldsymbol{g}$-direction; and a linear shear flow in the $\boldsymbol{B}_p\boldsymbol{g}$-direction, which arises only if $\boldsymbol{b}^{+} \neq \boldsymbol{b}^{-}$. Substituting (4.1) into (2.9), we find

$$\boldsymbol{A}_p = \boldsymbol{C} - \boldsymbol{D}(\boldsymbol{I} + \boldsymbol{C})^{-1}\boldsymbol{D} \quad \text{and} \quad \boldsymbol{B}_p = (\boldsymbol{I} + \boldsymbol{C})^{-1}\boldsymbol{D} \tag{4.2}$$

in terms of the sum and difference tensors defined in (3.3).

In the limit of no slip on the upper surface $\boldsymbol{b}^{+} = \boldsymbol{0}$, our solution reduces to that of Stone *et al.* (2004). In that case, $h\boldsymbol{C} = -h\boldsymbol{D} = \boldsymbol{b}^{-}$, the coefficient tensors, $\boldsymbol{A}_p$ and $\boldsymbol{B}_p$, and the permeability $\boldsymbol{K}$ are all coaxial with the slip-length tensor $\boldsymbol{b}^{-}$ of the lower surface. Here, we analyse more general situations where the upper and lower surfaces have different slip tensors.

For symmetric $\boldsymbol{b}^{\pm}$, we can diagonalize $\boldsymbol{A}_p$ and $\boldsymbol{B}_p$ in the same simple situations considered above for shear flow. In the case of aligned but different slip tensors (3.4),

https://doi.org/10.1017/S002211200800356X Published online by Cambridge University Press

the coefficient tensors (4.2) are diagonalized by the same rotation matrix:

$$\boldsymbol{A}_p = \boldsymbol{S}_\theta \begin{pmatrix} A_s(b_\parallel^+, b_\parallel^-) & 0 \\ 0 & A_s(b_\perp^+, b_\perp^-) \end{pmatrix} \boldsymbol{S}_{-\theta}, \tag{4.3}$$

$$\boldsymbol{B}_p = \boldsymbol{S}_\theta \begin{pmatrix} B_s(b_\parallel^+, b_\parallel^-) & 0 \\ 0 & B_s(b_\perp^+, b_\perp^-) \end{pmatrix} \boldsymbol{S}_{-\theta}, \tag{4.4}$$

and the eigenvalues

$$A_s(b^+, b^-) = \frac{b^+ + b^- + 4h^{-1}b^+b^-}{h + b^+ + b^-} \quad \text{and} \quad B_s(b^+, b^-) = \frac{b^+ - b^-}{h + b^+ + b^-} \tag{4.5}$$

result from scalar slip in the eigendirections. There are several simple cases: (i) if the surfaces are isotropic, $\boldsymbol{b}^\pm = b^\pm \boldsymbol{I}$, then $\boldsymbol{A}_p = A_s \boldsymbol{I}$ and $\boldsymbol{B}_p = B_s \boldsymbol{I}$; (ii) if the surfaces have the same slip tensors, $\boldsymbol{b}^+ = \boldsymbol{b}^- = \boldsymbol{b}$, then $\boldsymbol{A}_p = 2h^{-1}\boldsymbol{b}$ and $\boldsymbol{B}_p = \boldsymbol{0}$; (iii) if the upper surface has no slip, $\boldsymbol{b}^+ = \boldsymbol{0}$ and $\boldsymbol{b}^- = \boldsymbol{b}$, then $A_s = -B_s = b/(h + b)$, or more compactly $\boldsymbol{A}_p = -\boldsymbol{B}_p = \boldsymbol{b}(h\boldsymbol{I} + \boldsymbol{b})^{-1}$, which reduces our solution to that of Stone *et al.* (2004) for one textured surface.

For identical but misaligned textures (3.8), we find $\boldsymbol{A}_p = \boldsymbol{C}$ and $\boldsymbol{B}_p = \boldsymbol{0}$, using (3.9) and (3.10). Now the slip-driven shear flow vanishes by symmetry. The slip-driven plug flow is proportional to the average slip-length tensor and diagonalized by $\boldsymbol{S}_{\bar\theta}$, where $\bar\theta$ is the angle that bisects the surface orientation angles; a pressure gradient in this direction cannot produce any transverse flow, if the two textures are the same.

4.2. *Permeability*

In many situations, one is more interested in the depth-integrated total flow rate in a given direction than the velocity profile. In linear response, the depth-averaged velocity $\overline{\boldsymbol{u}}$ is proportional to the applied pressure gradient,

$$\overline{\boldsymbol{u}} = \frac{1}{h}\int_{-h/2}^{h/2} \boldsymbol{u}\, \mathrm{d}z = \boldsymbol{\kappa}\, \boldsymbol{g}, \tag{4.6}$$

via the permeability tensor $\boldsymbol{\kappa}$. For the anisotropic Poiseuille flow (4.1), this integral is easily performed to obtain

$$\boldsymbol{\kappa} = \frac{h^2}{12\eta}\boldsymbol{K}, \quad \text{where} \quad \boldsymbol{K} = \boldsymbol{I} + 3\boldsymbol{A}_p \tag{4.7}$$

is the dimensionless permeability, scaled to its value without slip. The permeability is generally enhanced by slip-driven plug flow in direction $\boldsymbol{A}_p\boldsymbol{g}$. (The slip-driven shear flow does not affect the permeability, although it contributes to mixing.)

The results above for $\boldsymbol{A}_p$ in various special cases can be extended to $\boldsymbol{K}$, since the two tensors are coaxial:

$$\boldsymbol{K} = \boldsymbol{S}_{\theta_K} \begin{pmatrix} K_\parallel & 0 \\ 0 & K_\perp \end{pmatrix} \boldsymbol{S}_{-\theta_K}, \tag{4.8}$$

where $\boldsymbol{S}_{\theta_K}$ diagonalizes $\boldsymbol{A}_p$ and $\boldsymbol{K}$. For aligned but different textures (3.4), the permeability has the same orientation as the textures, $\theta_K = \theta$, and its eigenvalues, $K_\parallel = K_s(b_\parallel^+, b_\parallel^-)$ and $K_\perp = K_s(b_\perp^+, b_\perp^-)$ correspond to cases of scalar slip,

$$K_s(b^+, b^-) = \frac{h + 4(b^+ + b^-) + 12h^{-1}b^+b^-}{h + b^+ + b^-}. \tag{4.9}$$

https://doi.org/10.1017/S002211200800356X Published online by Cambridge University Press

For identical but misaligned textures (3.8), the permeability is orientated with the mean angle $\theta_K = \bar{\theta} = (\theta^+ + \theta^-)/2$ with eigenvalues given by

$$K_\parallel = 1 + \frac{6}{h}(b_\parallel \cos^2 \Delta\theta + b_\perp \sin^2 \Delta\theta), \tag{4.10}$$

$$K_\perp = 1 + \frac{6}{h}(b_\parallel \sin^2 \Delta\theta + b_\perp \cos^2 \Delta\theta), \tag{4.11}$$

where $\Delta\theta = (\theta^+ - \theta^-)/2$. If $\Delta\theta = \pi/4$, then the permeability is isotropic, $\boldsymbol{K} = K\boldsymbol{I}$ with $K = K_\parallel = K_\perp = 1 + (3/h)(b_\parallel + b_\perp)$.

Microfluidic devices often contain thin channels of rectangular cross-section with parallel sidewalls at $y = \pm L$ with $L \gg h$. In that case, the mean downstream permeability of the channel, $\tilde{\kappa}_x = (h^2/12\eta)\tilde{K}_x$, defined by $\overline{u}_x = \tilde{\kappa}_x g_x$, can be easily derived from the permeability tensor $\boldsymbol{\kappa}$ defined in (4.6). Ignoring departures from Poiseuille flow within $O(h)$ of the sidewalls, the constraint of vanishing transverse flow, $\overline{u}_y = 0$, is maintained by an induced transverse pressure gradient, $g_y = -(\kappa_{yx}/\kappa_{yy})g_x$, which drives an additional anisotropic Poiseuille flow. Superimposing these flows, we obtain

$$\tilde{K}_x = K_{xx} - \frac{K_{xy}K_{yx}}{K_{yy}} = \frac{\det(\boldsymbol{K})}{K_{yy}} = \frac{K_\parallel K_\perp}{K_{yy}}. \tag{4.12}$$

The channel permeability can also be expressed in terms of an effective downstream slip length $\tilde{b}_x$ defined by $\tilde{K}_x = 1 + (6/h)\tilde{b}_x$, although this obscures the true tensorial nature of the hydrodynamic slip.

5. Conclusion

Our solutions for anisotropic flows between textured plates may be useful in interpreting experiments and simulations. As in the case of scalar Poiseuille flow, bulk velocity profiles can be fitted to the theory to systematically extract boundary effects of slippage and assess the validity of the tensorial slip hypothesis. Our results also allow the local slip tensors to be determined by global measurements, such as the permeability of a textured channel or the force required to shear textured plates, as a function of the surface orientations. In such measurements, departures from our predictions could be used to isolate nonlinear, inhomogeneous, or non-symmetric slip response, e.g. due to nanobubble deformation at superhydrophobic surface (Sbragaglia & Prosperetti 2007), surface curvature (Vinogradova 1995), or variable channel width (Lauga, Stroock & Stone 2004).

More generally, our calculations illustrate the power of the tensor formalism in capturing complicated effects of textured surfaces, while preserving simple fluid domains. The general boundary condition (2.2) may be useful in many other situations, such as lubrication flows between textured gears, spreading or drainage of thin films, dispersion and mixing in grooved channels (Stroock *et al.* 2002*a*,*b*), sedimention of textured particles (Lecoq *et al.* 2004), and electrokinetics of patterned surfaces (Ajdari 2002). Transverse spatial couplings could also be added to existing tensorial (but isotropic) slip boundary conditions for fluids with internal degrees of freedom, such as liquid crystals and polymer melts; anisotropic surface texture can influence molecular orientations and thus the effective slip (Heidenreich *et al.* 2007), which could have interesting consequences for theory and applications.

The authors gratefully acknowledge the hospitality of ESPCI and support by the Paris-Sciences Chair (M. Z. B.) and Joliot Chair (O. I. V.).

https://doi.org/10.1017/S002211200800356X Published online by Cambridge University Press

REFERENCES

Ajdari, A. 2002 Transverse electrokinetic and microfluidic effects in micropatterned channels: Lubrication analysis for slab geometries. *Phys. Rev.* E **65**, 016301.

Bocquet, L. & Barrat, J. L. 1994 Hydrodynamic boundary conditions, correlation functions, and kubo relations for confined fluids. *Phys. Rev.* E **49**, 3079–3092.

Bocquet, L. & Barrat, J. L. 2007 Flow boundary conditions from nano- to micro-scales. *Soft Matter* **3**, 685–693.

Choi, C. H., Ulmanella, U., Kim, J., Ho, C. M. & Kim, C. J. 2006 Effective slip and friction reduction in nanograted superhydrophobic microchannels. *Phys. Fluids* **18**, 087105.

Cottin-Bizonne, C., Barrat, J. L., Bocquet, L. & Charlaix, E. 2003 Low-friction flows of liquid at nanopatterned interfaces. *Nat. Mater.* **2**, 237–240.

Cottin-Bizonne, C., Cross, B., Steinberger, A. & Charlaix, E. 2005 Boundary slip on smooth hydrophobic surfaces: Intrinsic effects and possible artifacts. *Phys. Rev. Lett.* **94**, 056102.

Einzel, D., Panzer, P. & Liu, M. 1990 Boundary-condition for fluid-flow – curved or rough surfaces. *Phys. Rev. Lett.* **64**, 2269–2272.

Heidenreich, S., Ilg, P. & Hess, S. 2007 Boundary conditions for fluids with internal orientational degrees of freedom: Apparent velocity slip associated with the molecular alignment. *Phys. Rev.* E **75**, 066302.

Hess, S. & Loose, W. 1989 Slip flow and slip boundary coefficient of a dense fluid via nonequilibrium molecular dynamics. *Physica* A **162**, 138–144.

Joly, L., Ybert, C. & Bocquet, L. 2006 Probing the nanohydrodynamics at liquid-solid interfaces using thermal motion. *Phys. Rev. Lett.* **96**, 046101.

Joseph, P., Cottin-Bizonne, C, Benoĭ, J. M., Ybert, C., Journet, C., Tabeling, P. & Bocquet, L. 2006 Slippage of water past superhydrophobic carbon nanotube forests in microchannels. *Phys. Rev. Lett.* **97**, 156104.

Lauga, E., Brenner, M. P. & Stone, H. A. 2007 *Handbook of Experimental Fluid Dynamics*, chap. 19, pp. 1219–1240. Springer.

Lauga, E., Stroock, A. D. & Stone, H. A. 2004 Three-dimensional flows in slowly varying planar geometries. *Phys. Fluids* **16**, 3051–3062.

Lecoq, N., Anthore, R., Cichocki, B., Szymczak, P. & Feuillebois, F. 2004 Drag force on a sphere moving towards a corrugated wall. *J. Fluid Mech.* **513**, 247–264.

Navier, C. L. M. H. 1823 Mémoire sur les lois du mouvement des fluides. *Mém. l'Acad. R. Sci. lÍnst. France* **6**, 389–440.

Ou, J. & Rothstein, J. P. 2005 Direct velocity measurements of the flow past drag-reducing ultrahydrophobic surfaces. *Phys. Fluids* **17**, 103606.

Quéré, D. 2005 Non-sticking drops. *Rep. Prog. Phys.* **68**, 2495–2532.

Sbragaglia, M. & Prosperetti, A. 2007 A note on the effective slip properties for microchannel flows with ultrahydrophobic surfaces. *Phys. Fluids* **19**, 043603.

Squires, T. M. & Quake, S. R. 2005 Microfluidics: Fluid physics at the nanoliter scale. *Rev. Mod. Phys.* **77**, 977.

Stone, H. A., Stroock, A. D. & Ajdari, A. 2004 Engineering flows in small devices. *Annu. Rev. Fluid Mech.* **36**, 381–411.

Stroock, A. D., Dertinger, S. K. W., Ajdari, A., Mezić, I., Stone, H. A. & Whitesides, G. M. 2002*a* Chaotic mixer for microchannels. *Science* **295**, 647–651.

Stroock, A. D., Dertinger, S. K., Whitesides, G. M. & Ajdari, A. 2002*b* Patterning flows using grooved surfaces. *Anal. Chem.* **74**, 5306–5312.

Vinogradova, O. I. 1995 Drainage of a thin liquid film confined between hydrophobic surfaces. *Langmuir* **11**, 2213–2220.

Vinogradova, O. I. 1999 Slippage of water over hydrophobic surfaces. *Intl J. Miner. Proc.* **56**, 31–60.

Vinogradova, O. I., Bunkin, N. F., Churaev, N. V., Kiseleva, O. A., Lobeyev, A. V. & Ninham, B. W. 1995 Submicrocavity structure of water between hydrophobic and hydrophilic walls as revealed by optical cavitation. *J. Colloid Interface Sci.* **173**, 443–447.

Vinogradova, O. I. & Yakubov, G. E. 2003 Dynamic effects on force measurements. 2. lubrication and the atomic force microscope. *Langmuir* **19**, 1227–1234.

Wang, C. Y. 2003 Flow over a surface with parallel grooves. *Phys. Fluids* **15**, 1114–1121.

https://doi.org/10.1017/S002211200800356X Published online by Cambridge University Press